Lawrence Berkeley National Laboratory
Recent Work

Title

II. THE CHARACTERIZATION OF MULTILAYER X-RAY ANALYZERS - MODELS AND MEASUREMENTS

Permalink

https://escholarship.org/uc/item/9sj1t467

Author

Henke, B.L.

Publication Date

1986-08-01

eScholarship.org Powered by the California Digital Library
University of California

LBL-21003
Preprint
c.2

Lawrence Berkeley Laboratory

UNIVERSITY OF CALIFORNIA

RECEIVED
LAWRENCE
BERKELEY LABORATORY

OCT 2 1986

LIBRARY AND
DOCUMENTS SECTION

Accelerator & Fusion Research Division

Submitted to Optical Engineering

II. THE CHARACTERIZATION OF MULTILAYER X-RAY ANALYZERS - MODELS AND MEASUREMENTS

B.L. Henke, J.Y. Uejio, H.T. Yamada, and
R.E. Tackaberry

August 1986

TWO-WEEK LOAN COPY
This is a Library Circulating Copy
which may be borrowed for two weeks

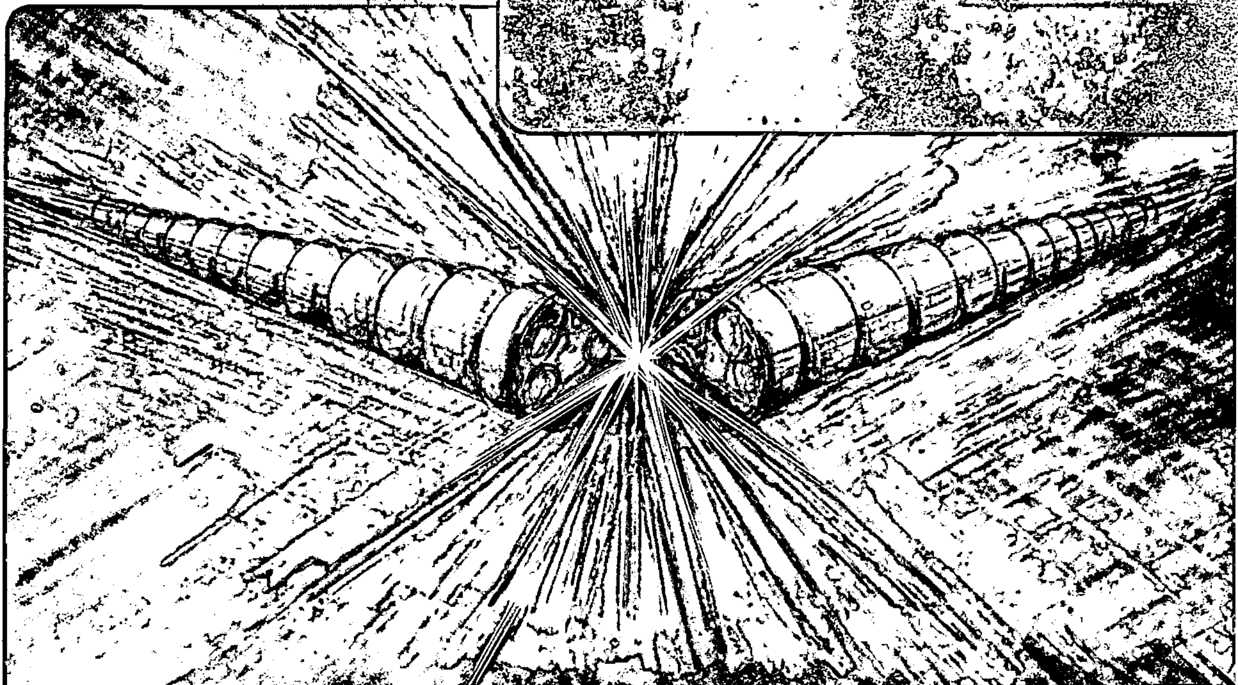

Prepared for the U.S. Department of Energy under Contract DE-AC03-76SF00098

LBL-21003
c.2

DISCLAIMER

This document was prepared as an account of work sponsored by the United States Government. While this document is believed to contain correct information, neither the United States Government nor any agency thereof, nor the Regents of the University of California, nor any of their employees, makes any warranty, express or implied, or assumes any legal responsibility for the accuracy, completeness, or usefulness of any information, apparatus, product, or process disclosed, or represents that its use would not infringe privately owned rights. Reference herein to any specific commercial product, process, or service by its trade name, trademark, manufacturer, or otherwise, does not necessarily constitute or imply its endorsement, recommendation, or favoring by the United States Government or any agency thereof, or the Regents of the University of California. The views and opinions of authors expressed herein do not necessarily state or reflect those of the United States Government or any agency thereof or the Regents of the University of California.

II. THE CHARACTERIZATION OF MULTILAYER X-RAY ANALYZERS - MODELS AND MEASUREMENTS*

B.L. Henke, J. Y. Uejio, H. T. Yamada and R. E. Tackaberry

Center for X-Ray Optics
University of California
Lawrence Berkeley Laboratory
Berkeley, California 94720

ABSTRACT

A procedure is described for a detailed characterization of multilayer analyzers which can be effectively applied to their design, optimization and application for absolute x-ray spectrometry in the 100-10,000 eV photon energy region. An accurate analytical model has been developed that is based upon a simple modification of the dynamical Darwin-Prins theory to extend its application to finite multilayer systems and to the low-energy x-ray region. Its equivalence to the optical E&M solution of the Fresnel equations at each interface is demonstrated by detailed comparisons for the reflectivity of a multilayer throughout the angular range of incidence of 0 to 90°. A special spectrograph and experimental method is described for the measurement of the absolute reflectivity characteristics of the multilayer. The experimental measurements at three photon energies in the 100-2000 eV region are fit by the analytical modified Darwin-Prins equation (MDP) for $I(\theta)$, generating a detailed characterization of two "state of the art" multilayers, of sputtered tungsten-carbon with $2d \approx 70$ A and of a molecular lead stearate with $2d \approx 100$ A. The fitting parameters that are determined by this procedure are applied to help establish the structural characteristics of these multilayers.

Subject terms: low energy x-rays; x-ray spectroscopy, x-ray reflection; sputtered/evaporated multilayers; Langmuir-Blodgett multilayers

*To be published in Optical Engineering (August, 1986)

I. INTRODUCTION

The x-ray physics and technology have been considerably advanced in the last decade as demanded for the development and application of the new, high intensity x-ray generating sources of synchrotron and high temperature plasma radiations. These have important applications, for example, in the material sciences and in the research and development of fusion energy and now of the x-ray lasers. Along with these developments has arisen a considerable need for accurate, absolute x-ray spectrometry.

For efficient x-ray analysis in the 100-10,000 eV region (1-100 A range) an important class of analyzers may be applied that utilize Bragg reflection from periodic layer structures which are parallel to the analyzer surface. These analyzers can be constructed in sufficiently thin sections to allow their effective application with curved, focussing optics. We define these analyzer systems generally to be <u>multilayers</u> of the natural or synthesized <u>molecular</u> types and of the synthesized <u>sputtered-or-evaporated</u> types. Examples of the molecular analyzers that we have used effectively in the 100-10,000 eV region (with 2d values of 3-160 A) are LiF, PET, mica (at third and first orders), the acid phthalates and the Langmuir-Blodgett multilayers (1,2). The sputtered/evaporated types have been "tailored" in the 2d range of 20 to several hundred angstroms (3,4,5) of high and low Z layers chosen from a large group of possible combinations (7). We would generally compare the Langmuir-Blodgett molecular analyzers as having lower atomic densities, lower integrated reflectivities, similar peak reflectivities, and higher resolution than do the high density, more rugged sputtered/evaporated multilayers of the same d-spacing. Both types have important application advantages in modern spectroscopy and are definitely complementary.

In order to efficiently design, optimize and apply the multilayer analyzers for a given spectroscopic measurement it is of considerable advantage to have a fast, flexible and accurate mathematical model code that describes the important reflectivity characteristics and can be accomodated on a small laboratory computer that may be associated with the spectrographic equipment. We have developed such a mathematical model for multilayer analyzers and apply it here to yield a detailed characterization of two "state of the art" large d-spacing analyzers: a sputtered tungsten-carbon analyzer (2d $\approx$ 70 A) and a molecular lead stearate analyzer (2d $\approx$ 100 A).

II. AN ANALYTICAL DESCRIPTION OF MULTILAYER REFLECTIVITY FOR THE 100-10,000 eV REGION

We present here an analytical expression for the intensity, I, that is reflected from a system of N periodic layers for incident angles, θ, throughout the 0 to 90 degree range. It has been obtained by modifying the dynamical theory of Darwin-Prins (for reflection from an ideal crystal of an infinite number of layers) to obtain a description for N-layer finite crystal reflection for all angles of Bragg and total reflection and for the x-ray region of 100-10,000 eV. We intend this approach to complement that of the optical E&M boundary value solution at each interface of the Fresnel equations (7,8). In the optical E&M wave solution (OEM), the layer pairs are defined by pairs of their refractive indices ($n = 1 - \delta - i\beta$) and by the corresponding average values, $\bar{\delta}$ and $\bar{\beta}$, for the multilayer. In our modified Darwin-Prins description (MDP) the reflecting layer systems are described as planes of unit cells of structure factor F, ($= F_1 + iF_2$) and of average scattering factor, $\bar{f}$ ($= \bar{f}_1 + i\bar{f}_2$). In Fig. 1 we present the DP expressions for the amplitudes reflected and transmitted at an elementary plane of unit cells in terms of the parameters $\underline{s}$ and $\underline{\sigma}$ which have been related to $\bar{f}$ and F by using elementary physical optics (see, for example, Compton and Allison (9) and James (10)). In the DP description it is assumed that the fractional complex amplitude that is reflected, $\underline{s}$, and that absorbed, σ, by the unit cell plane are small as compared to unity (as is generally required for the practical multilayer analyzer for which the effective number of interacting planes is large).

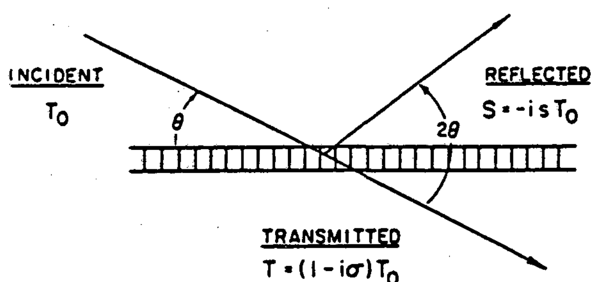

FOR m UNIT CELLS/UNIT AREA OF STRUCTURE FACTOR, $F_1 + iF_2$, AND OF AVERAGE SCATTERING FACTOR, $\bar{f}_1 + i\bar{f}_2$, PER UNIT CELL

$$\sigma = mr_0\lambda \frac{\bar{f}_1 + i\bar{f}_2}{\sin\theta} \quad \text{AND} \quad S = mr_0\lambda \frac{F_1 + iF_2}{\sin\theta} P(2\theta)$$

$P(2\theta)$ = 1 OR COS 2θ FOR THE TWO POLARIZED COMPONENTS

Figure 1. Defining the small absorption and reflection amplitude fractions, σ and s, at each plane of unit cells of the multilayer in terms of the average scattering factor, $\bar{f}$, the structure factor, F, for the unit cell and their area density, m.

In the dynamical description of the propagation of waves through the multilayer all possible multiple reflections within the layers must be taken into account in order to describe the net downward propagating wave amplitude, $\underline{T}$, and the net upward propagating wave amplitude, $\underline{S}$. This accounting has been elegantly accomplished by Darwin in his solution of the self-consistent difference equations describing the process for any two adjacent layers within the semi-infinite multilayer (9,10). This approach yields the analytical result for the ratio of the reflected to the incident amplitudes, S_0/T_0, at the surface of the semi-infinite multilayer which is given by:

$$S_0/T_0 = \frac{-s}{(\sigma + \xi) \mp \sqrt{(\sigma + \xi)^2 - s^2}} \tag{1}$$

The third parameter, ξ, introduced in this result, is defined by:

$$\xi = \frac{2\pi}{\lambda} d(\sin\theta - \sin\theta_0) \tag{2}$$

where, as discussed below, $\sin\theta_0$ effectively defines a "region of interest" (given by the Bragg equation, $m\lambda = 2d\sin\theta_0$). Now, in this DP difference equation solution, it is established that the net downward propagating wave at the Nth layer has an amplitude given simply by $T_0 x^N$, where x is defined by:

$$x = (-1)^m \exp(-\eta) \tag{3}$$

$$\text{and } \eta = \mp\sqrt{s^2 - (\sigma + \xi)^2}$$

The value of x is the result of the contributing effects of all possible multiple reflections within the semi-infinite multilayer. (In η, the sign + or - is chosen to have its real part be positive.) Using this result, we derive here (in Appendix A), a modifying factor to be applied to the reflected amplitude ratio, S_0/T_0, given in Eq. (1) for the semi-infinite multilayer to obtain the required amplitude reflection ratio, S_{0N}/T_0, for the finite multilayer of N layers. This is given by:

$$S_{0N}/T_0 = (S_0/T_0)\,(1 - x^{2N})/(1 - (S_0/T_0)^2 x^{2N}) \tag{4}$$

Also derived in Appendix A is the amplitude ratio, T_{0N}/T_0, that is transmitted through the N layer system. This is given by:

$$T_{0N}/T_0 = [1-(S_0/T_0)^2]x^N/(1-(S_0/T_0)^2x^{2N}) \quad (5)$$

In the usual way, the intensity ratio that is reflected or transmitted for unpolarized incident x-radiation is obtained by taking one-half of the sum of the moduli squared of the two polarization component amplitudes as obtained from Eq. (4) and (5), by setting $P(2\theta)$ equal to unity and to $\cos 2\theta$.

As may be easily shown, the reflected intensity will be large only when the parameter, ξ, is small and therefore for the angular regions for which $\theta \approx \theta_0$ in this parameter, ξ. θ_0 is defined by the Bragg relation:

$$m\lambda = 2d \sin \theta_0 \quad (6)$$

($m = 0$ for the small angle, Fresnel reflection region, $m = 1$ for the first order diffraction line, $m = 2$ for the second order diffraction line, etc.) In order to apply this intensity function continuously for the total angular range, 0 to 90°, we automatically set m to be that integer which is nearest to the value of ($2d \sin \theta/\lambda$) in our code.

By using a structure factor, F, and an average value of the atomic scattering factor, $\bar{f}$, calculated by relations given in the next section, we have applied this modified Darwin-Prins result (MDP) to calculate the $I(\theta)$ for a sharply defined, pure tungsten/carbon multilayer of d-spacing = 35 A and with $\Gamma = 0.4$ (Γ is the ratio of the heavy layer thickness to the total d thickness of the layer pair.) A plot of $I(\theta)$ for the incident photons of Cu-Lα (930 eV/13.3 A) which includes the small angle Fresnel region and the first order diffraction line is shown in Fig. 2 for a number of layer pairs, N = 100. In Figs. 3 and 4 we compare, in

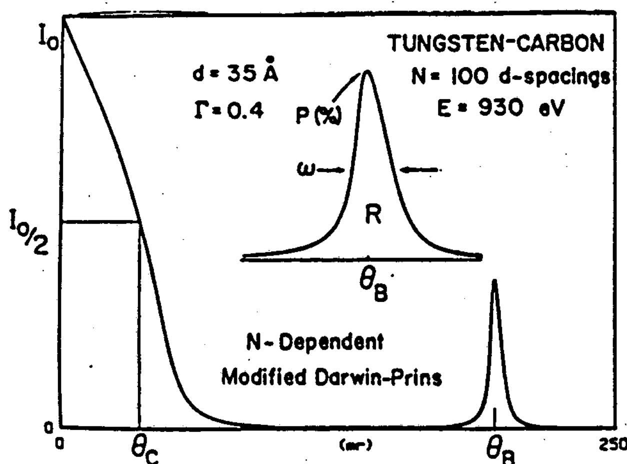

Figure 2. An MDP calculated reflectivity curve for 930 eV photons upon a tungsten-carbon multilayer of 2d = 70 A and with a sharply defined tungsten layer of thickness equal to Γd, with $\Gamma = 0.4$, N = 100. In the corresponding experimentally measured reflectivity curve, four characteristic values are determined for each photon energy, the total reflection cut-off angle, θ_C (at $I_0/2$), the integrated reflectivity, R, peak reflectivity, P, and FWHM, ω, at one or more diffraction orders.

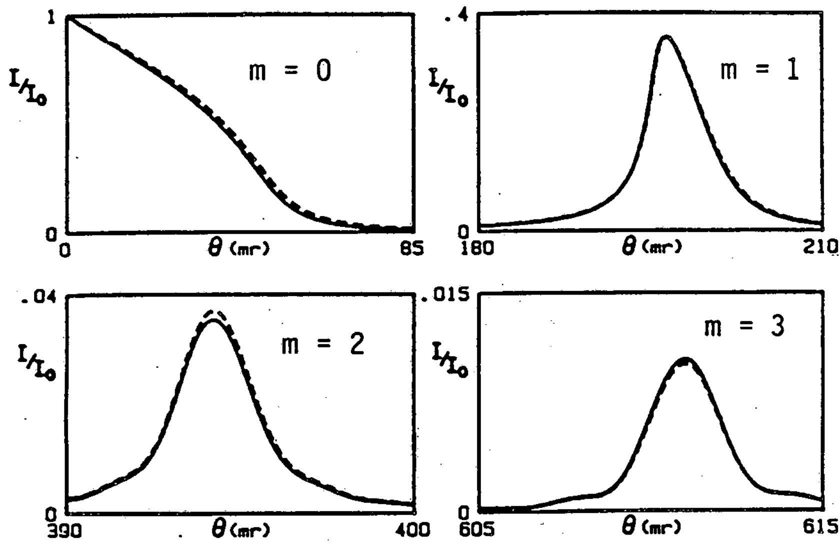

Figure 3. Comparing the MDP calculated reflectivity of the multilayer described in Fig. 2 with that calculated by the optical E&M model (dashed lines) for the total reflection region and for the first three diffraction orders.

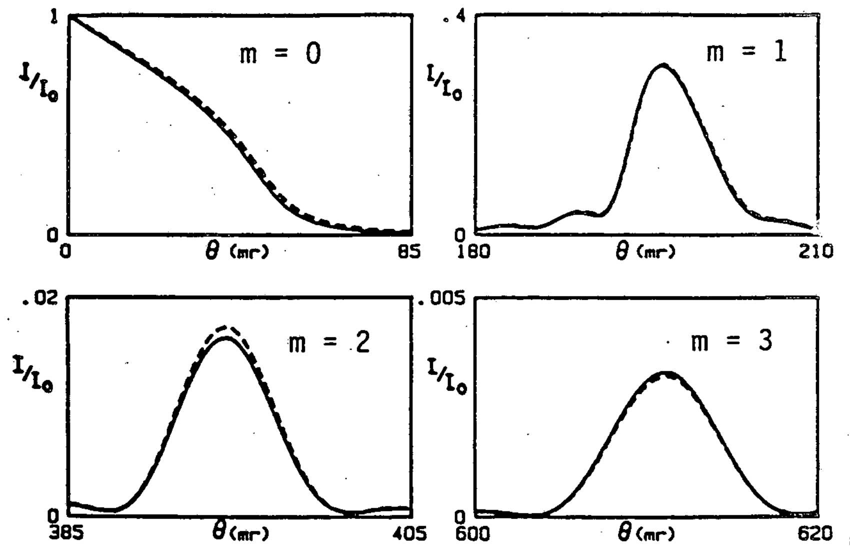

Figure 4. Detailed calculation comparisons as for Fig. 3 but with N = 30. (OEM - dashed lines)

detail, the total reflection region and the first, second and third order diffraction line intensities for this W/C multilayer as calculated by this MDP model to those as calculated by the optical E&M (OEM) model (dashed lines) for N = 100 and 30 in order to illustrate the equivalence of the two models in this low energy x-ray region. Similarly, we compare in Fig. 5 the intensities reflected by the multilayer of N = 100 at and near 90° (normal incidence). (OEM - dashed lines.)

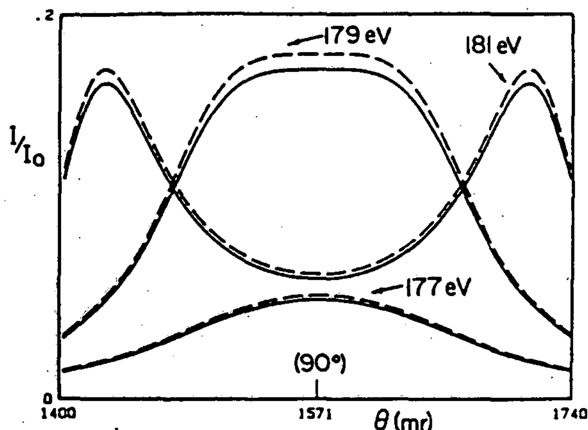

Figure 5. Detailed calculation comparisons as described for the 100 layer system of Fig. 2 but in the region of normal incidence. Note the sensitive "tuning" by varying the photon energy ∓ one percent from that yielding the maximum normal incidence reflectivity (OEM - dashed lines).

III. THE MEASUREMENT OF MULTILAYER REFLECTIVITY

The detailed characteristics of the multilayer reflection as predicted in Fig. 2 are experimentally measured by a specially designed vacuum spectrograph that is schematically described in Fig. 6. A fine slit and filter is positioned at the isolation gate window of one of our demountable x-ray tubes (11) to provide a strong, characteristic line source in the 100-10,000 eV region. The multilayer is mounted with its surface on the axis of a precision θ-2θ goniometer. A sharply defined incident beam is restricted to a small sampled region of the multilayer by a razor blade edge placed close to its surface. The angular resolution of the measurement is set by the divergence of the incident beam and essentially by the slit width at the x-ray source that is 120 cm from the goniometer axis. It is typically set to an angular resolution width that is small as compared to the diffraction line width of the multilayer analyzer. The reflected beam is measured by a sub-atmospheric, gas flow proportional counter with a window 10 cm from the goniometer axis and of width about one-third of that of the multilayer analyzer width and with a slit height that is large compared to that of the reflected beam. The effective incident beam is limited in width by the projection of the opening at the razor edge and is therefore proportional to <u>cos θ</u> as noted in Fig. 6.

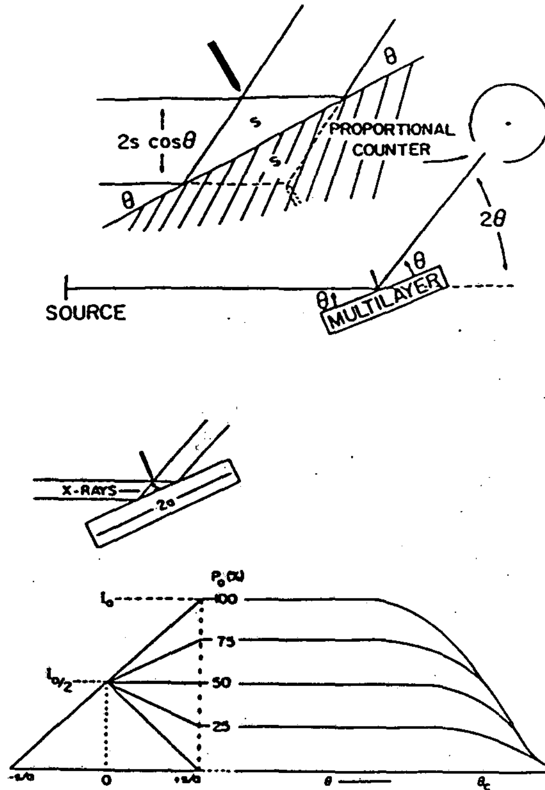

Figure 6. Illustrating the spectrograph geometry that is used for the measurement of multilayers reflectivity in the region of 0 to 70° and the characteristic inflection point in the intensity distribution at $\theta = 0$ and at $I_0/2$ (thereby defining the zero angle position of the goniometer and the incident intensity, $I_0 \cos\theta$). After the $I_0/2$ point the contribution of the reflected intensity causes a change in slope, which is greater as the real mirror reflectivity, P(%), for these small angles, departs from 100%.

After the onset of the measured Fresnel-reflection region and at $\theta = 0$, there usually appears an inflection point in the intensity at $I_0/2$ as illustrated in Fig. 6 (and in the experimental plots of Fig. 13). This onset feature determines the incident intensity, I_0, and the zero-angle position of the spectrograph.

The angular full-width-at-half-maximum (FWHM) of the diffraction line profile (in θ) may be simply determined in terms of the experimentally measured width, ω_x, the Gaussian instrumental width, g, and the Lorentzian emission line width, ε, by the following expression (12):

$$\omega = \omega_x\left(1-\left(\frac{g}{\omega_x}\right)^2\right)-\varepsilon \qquad (7)$$

where ε is given by:

$$\varepsilon = \frac{\Delta E}{E}\tan\theta_0 \qquad (8)$$

for which the x-ray source line of photon energy, E, has an effective energy width of ΔE.

The integrated reflectivity is determined by the total number of counts collected, N, as the diffraction line is scanned at an angular rate in θ of ω_0 by the relation (11):

$$R = \frac{\omega_0 N}{I_0 \cos\theta} \qquad (9)$$

The experimental peak reflectivity, P_x, is measured as the ratio of the intensity at the peak of the diffraction profile divided by the incident beam intensity, $I_0 \cos\theta$. Assuming that the shape of the true diffraction profile is essentially the same as that for the experimentally measured profile, the area under the profile, R, (integrated reflectivity) is equal to $K\omega P$ or $K\omega_x P_x$, where K is a shape factor. We may therefore obtain an estimate of true peak reflectivity, P, by the relation:

$$P = P_x \omega_x / \omega \qquad (10)$$

Note: It is required that the I_0 value used in these measurements be for only those incident photons of energy that are within the characteristic line that is being measured. Low energy background photons can usually be eliminated by an appropriate filter. The high energy photon background is effectively eliminated by the pulse height discrimination of the proportional counter. For our measurements, the Fresnel-reflection region through several orders of diffraction lines are measured at appropriate, normalized x-ray intensities, recorded and displayed with a multi-channel analyzer (MCA). This spectrum along with the associated pulse height spectrum for the detector provide an accurate check on the possible presence of any significant background radiation that may need to be further eliminated literally or by correction. The MCA is programmed to permit an immediate determination for each diffraction line of its centroid position, θ_x, FWHM, ω_x, peak reflectivity, P_x, and integrated reflectivity, R. These data and the spectra are transferred from the MCA to a small computer for the final semi-empirical characterization of the multilayer.

IV. FITTING THE MDP MODEL TO EXPERIMENTAL MEASUREMENTS

In order to obtain an absolute, detailed characterization of a given multilayer using the MDP model it is required to define for the unit cell its average scattering factor, $\bar{f}$, and the structure factor, F, thereby determining the $\underline{\sigma}$ and $\underline{s}$ material parameters of the MDP intensity

relations. These may be determined using an appropriate unit cell model and by requiring that the result, $I(\theta)$, precisely fits the experimental data for several photon energies at the characteristic values of R, P and ω for several diffraction orders (defined in Fig. 2). We will illustrate this procedure for the characterization of two types of multilayers, the sputtered tungsten-carbon multilayer and the molecular Langmuir-Blodgett multilayer.

A. Characterization of a Sputtered W/C Multilayer

We shall assume that a transition layer of both tungsten and carbon atoms may exist between pure tungsten and pure carbon regions of the multilayer as depicted in the unit cell model shown in Fig. 7 (Such a transition-layer model may be applied to account, for example, for an interface roughness (13) or a uniform distribution of W and C.) We shall assume here that this transition layer may be described as the chemically bonded compound, WC, as suggested by Auger electron analyses of W/C multilayers (14).

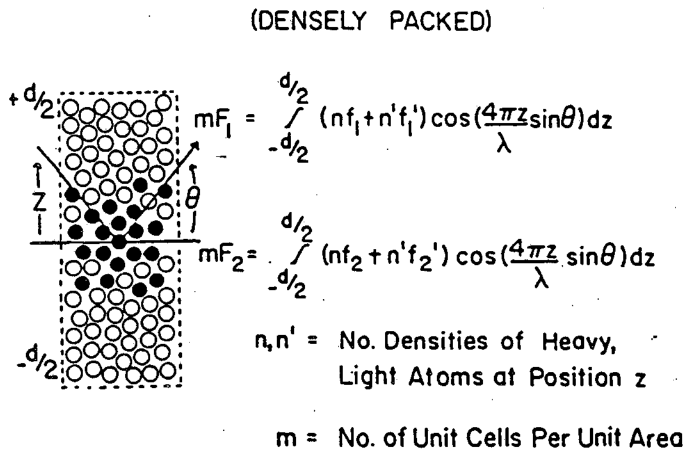

Figure 7. The symmetric unit cell that has been chosen to model a two element sputtered/evaporated, high atomic density multilayer with the possibility of having a transition layer interface structure. With N relatively large, the effects of fractional layers at the multilayer surfaces and of a substrate are usually negligible. Defined here are the general integrals for F_1 and F_2 for any symmetrical distribution of the heavy and light elements, $n(z)$ and $n'(z)$.

For such a uniform transition layer model, the mass per unit area for the light x-component (C), M_x, and the mass per unit area for the heavy y-component (W), M_y, that is originally deposited in the construction of each layer may be related to the mass densities, ρ_x, ρ_y and ρ_z, and to the fractional thicknesses, Γ_y and Γ_z, for the y (W) and z (WC) components as follows:

$$M_x = (1 - \Gamma_y - \Gamma_z)\rho_x d + \Gamma_z \rho_z d(A_x/A_z) \quad (11)$$

$$M_y = \Gamma_y \rho_y d + \Gamma_z \rho_z d(A_y/A_z) \quad (12)$$

where d is the thickness of the layered system and A_x, A_y and A_z are the atomic or molecular weights. And for the generalized symmetric description shown in Fig. 7, $(1 - \Gamma_y - \Gamma_z)d$, $\Gamma_y d$ and $\Gamma_z d$ are the total thicknesses of the carbon, tungsten and tungsten carbide layers, respectively. We estimate the mass densities ρ_x (for amorphous carbon), ρ_y (tungsten) and ρ_z (tungsten carbide) to be 2.0, 19.3 and 15.6 gm/cc respectively.

For this WC transition layer model, as suggested in the relations presented in Eq. (11), accurately known values of M_x and M_y along with those for the d-spacing and the mass densities, ρ_x, ρ_y and ρ_z, will allow the determination of the structural parameters, Γ_y and Γ_z. ($\Gamma_x = 1 - (\Gamma_y + \Gamma_z)$). These, in turn, may be applied to determine the average scattering factor, $m\bar{f}$, and the structure factor, mF, per unit area of the unit cell layer depicted in Fig. 1 and therefore to determine the essential optical parameters, σ and s. Usually, however, the amounts of the light and heavy elements that are deposited per unit area, M_x and M_y, are not accurately known and, as described below, these values or their equivalent parameters, Γ_y and Γ_z, are determined by fitting the model reflectivity relations to measured reflectivity data.

The structure factor, mF, per unit area of the unit cell layer ($F = F_1 + iF_2$) is defined by the following integral (derived from the general integrals presented in Fig. 7):

$$mF_i = \left[2n_y f_{iy} \int_0^{\frac{\Gamma_y d}{2}} \cos\left(\frac{4\pi z \sin\theta'}{\lambda'}\right) dz + 2n_z f_{iz} \int_{\frac{\Gamma_y d}{2}}^{\left(\frac{\Gamma_y + \Gamma_z}{2}\right)d} \cos\left(\frac{4\pi z \sin\theta'}{\lambda'}\right) dz + 2n_x f_{ix} \int_{\left(\frac{\Gamma_y + \Gamma_z}{2}\right)d}^{\frac{d}{2}} \cos\left(\frac{4\pi z \sin\theta'}{\lambda'}\right) dz\right] \qquad (13)$$

letting i = 1 or 2 for the real and imaginary components. Here m is the number of unit cells/ unit area, as applied in defining σ and s in Fig. 1.

The average scattering factor, $m\bar{f}$, per unit area of the unit cell layer is equal to that value of mF for forward scattering for which all atoms are scattering in phase and their scattering amplitudes add directly. Thus $m\bar{f} = mF$ for $\theta = 0$, and we obtain from Eq. (13):

$$m\bar{f}_1 = n_x f_{1x} \Gamma_x d + n_y f_{1y} \Gamma_y d + n_z f_{1z} \Gamma_z d \qquad (14)$$

and

$$m\bar{f}_2 = n_x f_{2x} \Gamma_x d + n_y f_{2y} \Gamma_y d + n_z f_{2z} \Gamma_z d \qquad (15)$$

Here n_x, n_y and n_z are the number of atoms or molecules per unit volume of atomic or molecular scattering factors, $f_{1x}+if_{2x}$, $f_{1y}+ if_{2y}$ and $f_{1z}+if_{2z}$, respectively.

$$(n_x = \frac{N_o \rho_x}{A_x},\ n_y = \frac{N_o \rho_y}{A_y} \text{ and } n_z = \frac{N_o \rho_z}{A_z}$$

where N_0 is Avagadro's No. and A_x, A_y and A_z are the atomic or molecular weights.)

Inside the multilayer, as a result of refraction, the angle of incidence and the wavelength at a unit cell plane must be the refraction modified values, θ' and λ'. The angle of refraction, θ' and the modified wavelength, λ', which must be used in the description of the wave interference within the multilayer are given by Snell's Law, $\cos\theta/\cos\theta' = 1 - \delta = \lambda/\lambda'$. We use here only the real part of the refractive index, $1 - \delta$, because it can be shown that for x-ray refraction effects the first order terms in β cancel. In the model description of multilayers in the low energy x-ray region where refraction effects become significant, we replace the ratio, $\sin\theta/\lambda$ which appears in the structure factor, F, by $\sin\theta'/\lambda'$ (in the cosine function of Eq. (13)). In terms of θ and λ, we may easily obtain from Snell's law the relation:

$$\frac{\sin\theta'}{\lambda'} = \frac{\sin\theta}{\lambda}\sqrt{1 - \frac{2\delta - \delta^2}{\sin^2\theta}} \qquad (16)$$

where $\delta = \frac{r_o \lambda^2 m}{2\pi d}\bar{f}_1$

Eq. (13) is integrated to yield:

$$mF_i = (n_y d f_{iy}/\kappa)\sin(\kappa\Gamma_y) + (n_z d f_{iz}/\kappa)[\sin(\kappa(\Gamma_y+\Gamma_z)) - \sin(\kappa\Gamma_y)] + (n_x d f_{ix}/\kappa)[\sin\kappa - \sin(\kappa(\Gamma_y+\Gamma_z))] \qquad (17)$$

where $\kappa = \frac{2\pi d \sin\theta'}{\lambda'}$ and letting $i = 1$ or 2 for the real and imaginary components.

Note: Because multilayer analyzers normally have a relatively large number of layers, N, to produce the desired resolution, it is usually sufficiently precise to model the analyzer by N layers of symmetric unit cells as defined in Fig. 7. The reflection effects of fractional layers at the boundaries and of a substrate can usually be considered negligible.

We fit our analytical model to the experimental integrated reflectivities at three photon energies and at the first three diffraction orders, if present, by varying Γ_y and Γ_z. These fits are verified by comparing the calculated and the experimental secondary values of ω and P for the several diffraction orders. As noted above, M_x and M_y values are uniquely determined by the values of Γ_y, Γ_z and d (given ρ_x, ρ_y, and ρ_z). The absolute value of the d-spacing is obtained from the measured d_x values defined by the Bragg equation ($m\lambda = 2d_x \sin \theta$) using Eq. (16) to obtain the relation,

$$d_x = d\sqrt{1 - \frac{2\delta - \delta^2}{\sin^2\theta}} \approx d\left(1 - \frac{\delta}{\sin^2\theta} \ldots\right) \tag{18}$$

Here again we need to use only the real part of the complex refractive index, $1 - \delta$, because it may be shown that the terms involving β become negligibly small for the x-ray region of interest here. To calculate the absolute d-spacing, we simply linearly extrapolate a plot of the measured values of d_x vs $\csc^2\theta$, using the relation from Eq. (18), $d_x = d - \delta d \csc^2\theta$. An example of such a least squares fitting and extrapolation is shown in Fig. 8.

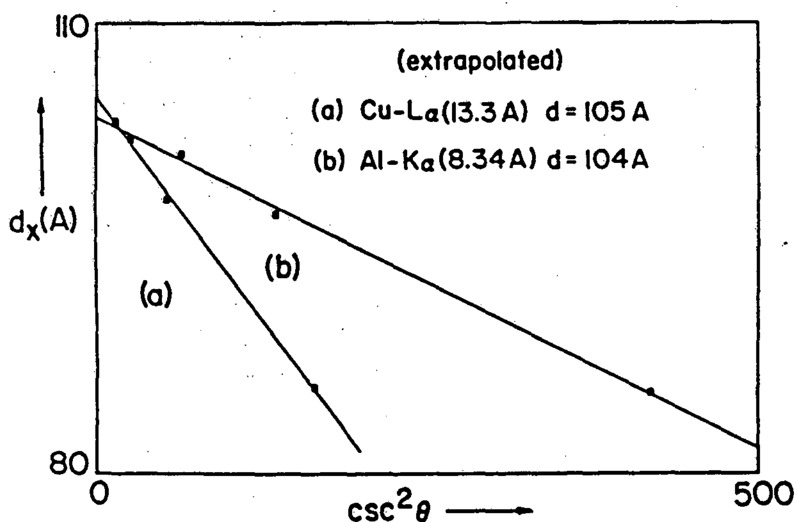

Figure 8. Determination of the absolute d-spacing for a W/C multilayer (N = 100) by an extrapolation of the d_x vs $\csc^2\theta$ plot for several diffraction orders, m, of the refraction relation:

$$d_x = d - (\delta d)\csc^2\theta$$

($d_x = m\lambda/2 \sin\theta$) The experimental values for the average optical constant, δ, for this multilayer as determined from the slopes of these linear plots are 1.12×10^{-3} and 4.24×10^{-4} for the wavelengths, 13.3 A and 8.34 A respectively.

For a determination of the atomic scattering factors, we have recently developed "state of the art" tables of f_1 and f_2 for Z = 1 to 94 and for photon energies 100-2000 eV (15). These tables have been established by numerically calculating atomic scattering factors using the Kramers-Kronig dispersion relations with our compilation of the available photoabsorption data above 30 eV. Using the numerical procedures and the photoabsorption data base from (15) these scattering

factor tables have recently been extended to 10,000 eV (16). These atomic scattering factors can be used to predict precisely the multilayer reflection characteristics but only for photon energies outside the regions near the absorption thresholds and above about 100 eV where the atoms within the solid can be expected to respond "atomic-like". Near the thresholds one may expect the photoabsorption to be strongly affected by molecular orbital resonances, EXAFS, etc. An example of a very dramatic threshold effect is the appearance of a strong and sharp reflectivity spike near the O-K edge (23.3 A) for the potassium acid phthalate (KAP) analyzer (17). Multilayer reflectivity at absorption edges should be determined by experimental measurement. Nevertheless, for the large extended regions in the 100-10,000 eV range, between absorption edges where the multilayer analyzers are normally applied, the atomic scattering description applied here should yield fairly accurate predictions.

Note: For only the low energy x-ray region (for which the wavelengths are large as compared to the dimensions of the atomic electron "cloud" around the nuclei) these atomic scattering factors may be considered angle-independent. For the wave reflection description within the multilayer for which the incident photon energies are higher (> 1000 eV) and/or for the large angles of reflection, a simple form-factor correction should be added to f_1, for these atomic scattering factors appearing in the structure factor, F. (A simple correction is described in Ref. (15).) Specifically, in the Darwin-Prins reflectivity expression, Eq. (1), the atomic scattering factors, f_1, in the forward-scattering parameter, σ, are for zero-angle scattering and require no form factor correction but those atomic scattering factors, f_1, in the parameter, s, describing scattering in the 2θ reflection direction, must be form-factor corrected. This correction is not included in the optical E&M (OEM) model because in this description it is assumed that the wavelengths are large as compared to atomic dimensions.

With standard fitting procedures, using experimental values for the integrated reflectivities for the multilayer at several photon energies and, if present, at several diffraction orders, along with the model relations Eqs. 14, 15 and 17, the mass per unit area values, M_x and M_y, and correspondingly the fractional thicknesses, Γ_y and Γ_z, may be determined. The $I(\theta)$ function thus determined may then be tested by comparing the predicted results with those measured for the Fresnel reflection characteristics and for the diffraction line profiles (P and ω) with those values as measured.

In Table 1 and in the plots of Fig. 9 we present the results of such a model fit for a typical sputtered tungsten-carbon multilayer (18). The present accuracy of the fitting by the MDP analytical function, $I(\theta)$, is indicated by the experimental points shown in the characterization plots of Fig. 9.

TABLE 1: CHARACTERIZATION OF A SPUTTERED TUNGSTEN-CARBON MULTILAYER

2d = 75 A N = 120 layers
Mass/area-layer, M_x = 0.46 µg/cm² M_y = 3.55 µg/cm²
Γ_x = 0.41 Γ_y = 0.19 Γ_z = 0.40

E(eV)	θ_c(mr)	θ_B(mr)	R(mr)	P(%)	ω(mr)	ΔE(eV)	E/ΔE	λ(A)
167.2	92.2	1570.8	27.94	9.04	270.52			74.1
171.7	89.1	1342.8	15.03	8.12	104.08	4.15	41	72.2
183.3	82.2	1149.5	5.06	6.57	53.47	4.39	42	67.6
192.6	78.4	1052.4	3.70	5.94	44.04	4.84	40	64.4
212.2	72.3	908.4	2.59	5.41	34.39	5.69	37	58.4
277.0	52.8	646.9	2.51	7.13	28.29	9.64	29	44.8
311.7	54.7	569.5	1.10	2.99	28.29	13.77	23	39.8
392.4	53.6	445.4	1.26	4.90	19.87	16.34	24	31.6
395.3	53.4	441.9	1.27	4.96	19.68	16.44	24	31.4
452.2	50.4	384.1	1.48	6.54	17.40	19.47	23	27.4
511.3	49.4	338.6	1.68	8.61	15.07	21.88	23	24.2
524.9	49.0	329.7	1.72	9.09	14.64	22.46	23	23.6
556.3	48.3	310.7	1.79	10.21	13.63	23.61	24	22.3
572.8	47.8	301.6	1.81	10.75	13.12	24.16	24	21.6
637.4	45.5	270.6	1.94	12.73	11.91	27.36	23	19.5
676.8	45.1	254.7	2.04	14.46	11.09	28.84	23	18.3
705.0	44.4	244.4	2.08	15.45	10.62	30.03	23	17.6
776.2	43.0	221.8	2.19	18.26	9.53	32.81	24	16.0
851.5	41.4	202.0	2.26	21.15	8.58	35.66	24	14.6
929.7	39.7	184.9	2.30	23.98	7.78	38.70	24	13.3
1011.7	37.9	169.8	2.32	26.77	7.09	41.83	24	12.3
1041.0	37.2	164.9	2.32	27.74	6.86	42.93	24	11.9
1188.0	34.1	144.4	2.26	32.07	5.89	48.15	25	10.4
1253.6	32.7	136.7	2.22	33.68	5.52	50.33	25	9.89
1486.7	28.0	115.0	1.91	37.65	4.30	55.38	27	8.34
1740.0	20.7	97.6	0.91	29.96	2.47	43.97	40	7.13

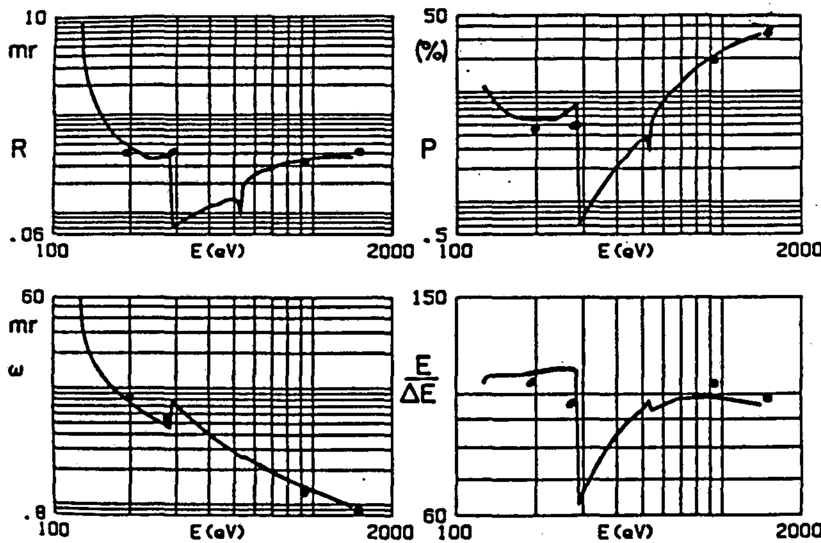

Figure 9. Plots of the integrated reflectivity, R(mrad), the peak reflectivity, P(%), the FWHM values, ω(mrad) and the resolving power, E/ΔE, for the sputtered W/C multilayer as characterized in Table 1. Presented here are the experimental determinations of these parameters at three x-ray lines, Mo-Mζ (192.6 eV/64.4 A), Cu-Lα (930 eV/13.3 A) and Al Kα (1487 eV/8.34 A).

In Table 2 are presented the measured values of the integrated reflectivities at the several photon energies and diffraction orders along with their ratios to the present fit values. Also presented here, for comparison, are their ratios to fit values determined by assuming sharp tungsten-carbon interfaces with no presence of transition layers. Suggested here is that a transition layer can account for the relative measured intensities for the several diffraction orders which are not predictable by a simple W/C model.

TABLE 2. Absolute Experimental Integrated Reflectivity Values at Several Diffraction Orders and Photon Energies. Comparisons to Corresponding Fit Values by the Transition Layer (W/WC/C) and the Pure (W/C) Models.

PHOTON ENERGY (eV)	DIFFRACTION ORDER	R(EXP) (mrad)	R(EXP) / R(W/WC/C)	R(EXP) / R(W/C)
192.6	1	4.20	1.13	1.10
929.7	1	2.04	0.886	0.873
929.7	2	.0196	0.927	0.291
929.7	3	.0137	1.13	0.360
1486.7	1	1.258	0.659	0.653
1486.7	2	.016	0.773	0.265
1486.7	3	.010	0.826	0.264

B. Characterization of a Molecular (LB) Multilayer

In Fig. 10 we define the structure factor, F, for a symmetric unit cell of a molecular multilayer. The scattering factor for this unit cell, $\bar{f}(= \bar{f}_1 + i\bar{f}_2)$, is given by the relations,

$$\bar{f}_1 = \Sigma n_q f_{1q} \qquad (19)$$

$$\bar{f}_2 = \Sigma n_q f_{2q}$$

Where n_q is the number of atoms of type q in the unit cell and having the atomic scattering factor, $f_{1q} + if_{2q}$.

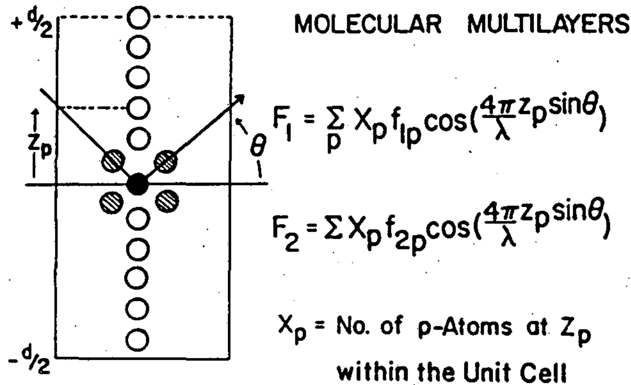

Figure 10. Defining the molecular structure factor components, F_1 and F_2, for a symmetric unit cell of a molecular multilayer.

For $m\bar{f}$ and mF values as needed to obtain σ and s (See Fig. 1), we may use $m = 1/A_0$ where A_0 is the cross-sectional area of the molecular unit cell.

In Fig. 11 is shown the molecular structure and the unit cell for the lead salt of the straight-chain fatty acids that are used in our construction of molecular analyzers of the Langmuir-Blodgett type. The general formula for the twenty molecules that can be used to generate Langmuir-Blodgett multilayers is $[CH_3(CH_2)_nCOO]_2Pb$. The d-spacing in the LB multilayer is approximately given by 2.50 (n + 4) A (20). We have constructed multilayers in the n = 10 to 28 range with 2d values of 70 to 160 A.

Figure 11. The unit cell structure for the lead salt of the straight-chain fatty stearic acid that comprises a molecular, Langmuir-Blodgett multilayer. Given this structure, the average atomic scattering factor, $\bar{f}$, and the structure factor, F, are determined.

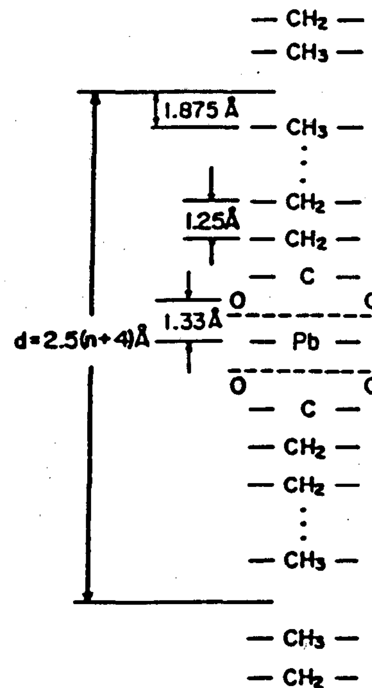

In order to fit the MDP analytical description to the experimental LB multilayer reflectivity we may adjust $\bar{f}$ and F by slightly varying the area density, m, (= $1/A_0$, A_0 the molecular cross-section) and the fraction, α, of the fatty acid molecules which have chemically combined with the lead ions to form the lead salt. It is easily shown that the latter adjustment is obtained by simply multiplying the scattering factor, f_{Pb}, for the lead atom by α where it appears in the calculation for $\bar{f}$ and F ($\alpha \approx 1$ and $A_0 \approx 20.5$ A^2, nominally). Again, the parameters A_0 and α are varied to obtain the "best fit" of the MDP results for the integrated reflectivities, R, at the first three diffraction orders (when present) and at several photon energies.

In Table 3 and in the associated Fig. 12 we present a detailed characterizations of a "state of the art" lead stearate analyzer (21). Also shown in these plots are the experimental measurements for R, P, ω, and E/ΔE at the three photon energies, 192.6 eV, 930 eV and 1487 eV.

TABLE 3: CHARACTERIZATION OF A MOLECULAR LEAD STERATE MULTILAYER

2d = 99 A N = 100 layers
A = 20.4 A^2 α = 0.8

E(eV)	θ_c(mr)	θ_B(mr)	R(mr)	P(%)	ω(mr)	ΔE(eV)	E/ΔE	λ(A)
125.3	141.8	1570.4	22.02	11.38	188.61			98.9
132.8	134.4	1233.6	2.83	9.41	26.47	1.23	108	93.4
148.7	120.9	1002.2	1.11	6.82	14.44	1.37	108	83.4
151.1	119.0	977.8	1.02	6.61	13.69	1.39	108	82.1
171.7	104.4	817.7	0.62	5.64	9.83	1.58	109	72.2
183.3	97.3	752.3	0.53	5.49	8.59	1.68	109	67.6
192.6	92.2	707.9	0.48	5.50	7.83	1.76	109	64.4
212.2	82.2	631.0	0.41	5.56	6.63	1.93	110	58.4
277.0	45.7	466.9	0.38	7.38	4.57	2.51	110	44.8
311.7	31.7	413.2	0.08	0.86	6.37	4.53	69	39.8
392.4	36.2	325.7	0.11	1.97	4.05	4.71	83	31.6
395.3	36.2	323.2	0.12	2.01	4.00	4.72	84	31.4
452.2	34.8	281.6	0.13	2.94	3.22	5.04	90	27.4
511.3	32.9	248.3	0.13	3.73	2.68	5.40	95	24.2
524.9	32.1	241.8	0.12	3.49	2.57	5.46	96	23.6
556.3	30.0	227.9	0.21	6.12	2.48	5.94	94	22.3
572.8	29.9	221.3	0.22	6.93	2.38	6.07	94	21.6
637.4	28.7	198.6	0.27	9.70	2.08	6.60	97	19.5
676.8	27.7	186.9	0.28	11.02	1.93	6.92	98	18.3
705.0	26.8	179.4	0.29	12.06	1.85	7.19	98	17.6
776.2	25.4	162.8	0.32	15.31	1.67	7.89	98	16.0
851.5	23.8	148.3	0.34	18.12	1.51	8.63	99	14.6
929.7	22.2	135.7	0.35	20.91	1.39	9.44	99	13.3
1011.7	20.8	124.7	0.36	23.87	1.28	10.34	98	12.3
1041.0	20.4	121.2	0.37	24.83	1.25	10.66	98	11.9
1188.0	18.2	106.1	0.37	29.01	1.10	12.31	97	10.4
1253.6	17.3	100.5	0.37	30.53	1.05	13.04	96	9.89
1486.7	14.8	84.7	0.35	34.99	0.90	15.68	95	8.34

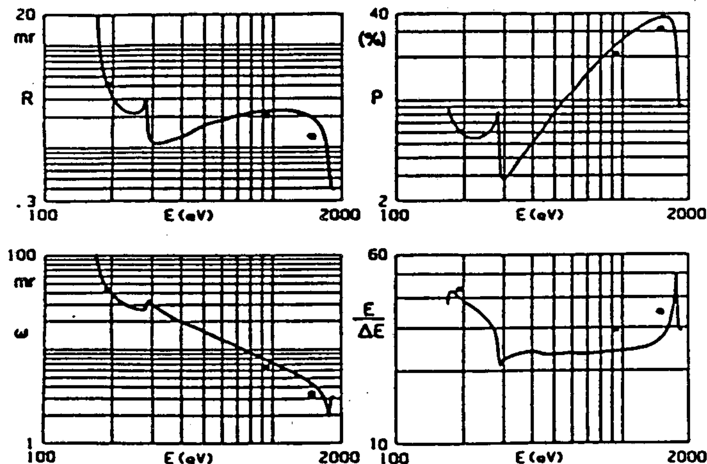

Figure 12. Plots for the integrated reflectivity, R(mrad), peak reflectivity, P(%), ω(mrad) and E/ΔE for the lead stearate molecular multilayer as characterized in Table 3. Experimentally determined points are also indicated here as for Fig. 9.

C. Reflectivity at Small Angles

In order to calculate the reflectivity at small angles, as noted earlier, we apply our MDP calculation for the region approaching θ equal to zero by setting m (= 2d sin θ_0/λ) equal to zero. For this small angle region of essentially only forward scattering, the values of the average scattering factor, $\bar{f}$, and the unit cell structure factor, F, approach the same value, and the DP parameters, σ and s, become essentially equal in this Fresnel reflection region. In this region the Darwin-Prins model and our Modified Darwin-Prins model can be easily shown to yield the Fresnel reflection equation depending only upon the optical constants, δ and β, providing that we make the substitutions for the average atomic scattering factor terms, $\bar{f}_1$ and $\bar{f}_2$, using the following relations:

$$\delta = \left(\frac{r_o\lambda^2 m}{2\pi d}\right)\bar{f}_1 \text{ and } \beta = \left(\frac{r_o\lambda^2 m}{2\pi d}\right)\bar{f}_2 \quad (20)$$

where r_o is the classical electron radius. These indeed are the usual equations relating the macroscopic optical constants, δ and β, to the atomic scattering parameters (e.g. see 9, 10, 15, 19).

Even at larger angles than those usually associated with a "total reflection" region, the Fresnel equation predicts a reflection tail which can be shown in this limit to become

$$I(\text{Fresnel}) \approx \frac{\delta^2 + \beta^2}{4\sin^4\theta} \quad \text{for } \theta >> \sqrt{2\delta} \quad (21)$$

In practice, this tail can be measured directly in the absence of any significant Bragg reflected lines. When the amplitude of a Bragg reflection is imposed, a distortion of this tail occurs as is illustrated in the measured spectra shown in Fig. 13 for two cases, with a first order diffracted line near and removed from the region of total

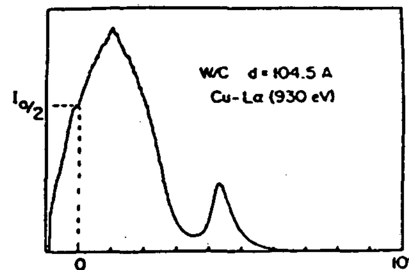

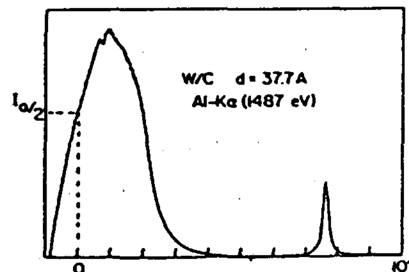

Figure 13. Illustrated here is the low-angle distortion of a spectral line that appears in the small-angle reflection region. Experimental spectra from W/C multilayers: (A) 2d = 200 A at Cu-L (13.3 A/930 eV) and (B) 2d = 70 A at Al-K (8.34 A/1487 eV).

reflection. As may be noted, the principal effect upon the shape of the diffraction line as it approaches the total reflection region is to distort the low angle side of the diffraction profile. It is for this reason that we have chosen as our definition for the measurement of the integrated reflectivity, R, and of the FWHM, ω_x, to measure only the area from the peak position on the large angle side (a range of 3 ω_x) and the associated one-half width, which values are then doubled to define R and ω_x. By this procedure, these values are different from those determined from the total profile only in the angles of Bragg diffraction near the total reflection region. We believe this definition of R and ω for the small angle region to be improved by this procedure as well as the speed of their computation.

It should be noted here that generally, for an optimized spectral measurement, a multilayer should be chosen with a 2d-value that places the spectrum at large Bragg angles. It is for these angles that the effect of the Fresnel reflection tail (combined effect for all wavelengths present) is minimized and maximum peak-to-background ratios are obtained. Also, for the larger angles of Bragg diffraction, the spectral resolution is less affected by the instrumental resolution which is usually fixed by sensitivity requirements and is angle-independent. The dispersion and the natural analyzer FWHM increase with the angle of diffraction.

The background enhancement at small angles is generally greater for the sputtered/evaporated multilayers as compared to that for the molecular multilayers because of their appreciably higher density and correspondingly higher δ and β values. This is illustrated in the measured spectra of Fig. 14 for the M-series of Molybdenum (the principal line, $M\zeta$, is at 64.4 A/192.6 eV.) These spectra are measured

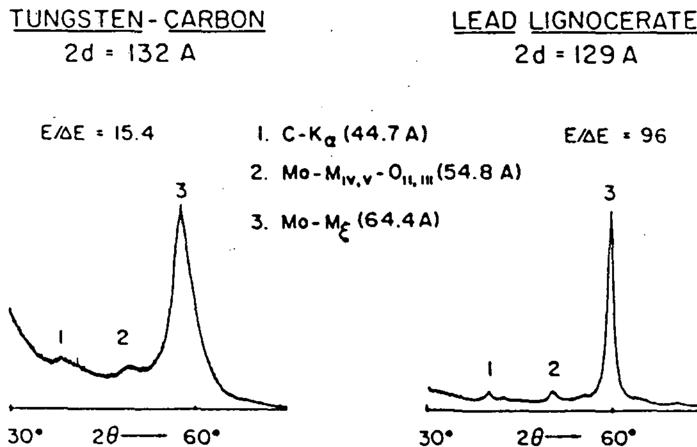

Figure 14. Comparing the experimental spectra for the Molybdenum-M series lines as measured with a sputtered W/C multilayer and with a molecular lead lignocerate multilayer, each of 2d ≈ 130 A.

with multilayers of the same 2d-values (≈ 130 A) of sputtered, tungsten/carbon and of the molecular lead lignocerate. Both were of effectively infinite thickness for this wavelength region. Comparative spectra as those shown in Fig. 14 usually demonstrate that the molecular multilayers of the same 2d-value have similar absolute peak reflectivities, higher resolving power and appreciably lower integrated reflectivities than do the higher higher density, sputtered/evaporated multilayer systems.

V. SUMMARY

A simple and accurate analytical model for the multilayer analyzer has been developed which can be effectively applied for the design, optimization and application of multilayers in absolute x-ray spectrometry. It may be applied for (1) finite systems of N layers and (2) for the low-energy as well as for the conventional x-ray region (100-10,000 eV). The structural detail of the multilayer is defined by a unit cell which, in turn, allows a determination of the model parameters which are the average scattering factor, $\bar{f}$, and of the structure factor, F, by simple mathematical formulae. These parameters along with m, the area density of the unit cells, are the only material parameters that are required for the MDP description.

By fitting the MDP model to the experimental measurements, as described here, we are able (1) to obtain a detailed analytical characterization of a given multilayer analyzer as based upon measurements at only a few photon energies, and (2) to gain some important insights as to the structure of the multilayer.

We are looking forward to improving the overall accuracy of the characterization procedures described here as we obtain multilayers of higher perfection, and more accurate photoabsorption data which are needed for the determination of the atomic scattering factors.

APPENDIX A - MDP FINITE MULTILAYER MODEL DERIVATION

As noted above, the Darwin-Prins (DP) solution for the ratio of the amplitude reflected to that incident, S_0/T_0, at the vacuum interface of a semi-infinite multilayer also established that the phase and effective attenuation of the net amplitude for a wave propagating into the semi-infinite crystal through N layers may simply be expressed as T_0x^N, x being given by the relation,

$$x = (-1)^m \exp(-\eta) \text{ where } \eta = \mp \sqrt{s^2-(\sigma+\xi)^2}$$

and is the result of the effects of all possible multiple reflections and transmissions occurring within the semi-infinite multilayer. (The + or - sign for η is chosen by the requirement that its real part be positive.)

The amplitude reflection ratio at the Nth layer, corresponding again to a boundary at an infinitely deep crystal, must also be S_0/T_0 and therefore the upward propagating wave amplitude at the Nth layer must be S_0x^N as depicted in Fig. A1 (A). In order to obtain the reflection ratio for a finite multilayer of N layers we need to eliminate the boundary condition of an effect of the wave interaction of the infinite mutilayer below the Nth layer. Let us reverse the roles of downward and upward waves in Fig. A1 (A) by inverting the reflection geometry of (A) as shown in (B). Now by multiplying each boundary wave amplitude indicated in (B) by the same constant factor, S_0x^N/T_0, we obtain another consistent set of values for the boundary wave amplitudes, as depicted in (C), with an incident wave from below of amplitude S_0x^N and which is equal to that in (A).

We now subtract, by a superposition, the two boundary wave solutions depicted in (A) and (C), obtaining the corresponding boundary amplitudes indicated in (D) and with the net upward propagating wave at the lower boundary equal to zero, the required boundary condition for the finite crystal of N layers.

Figure A-1.

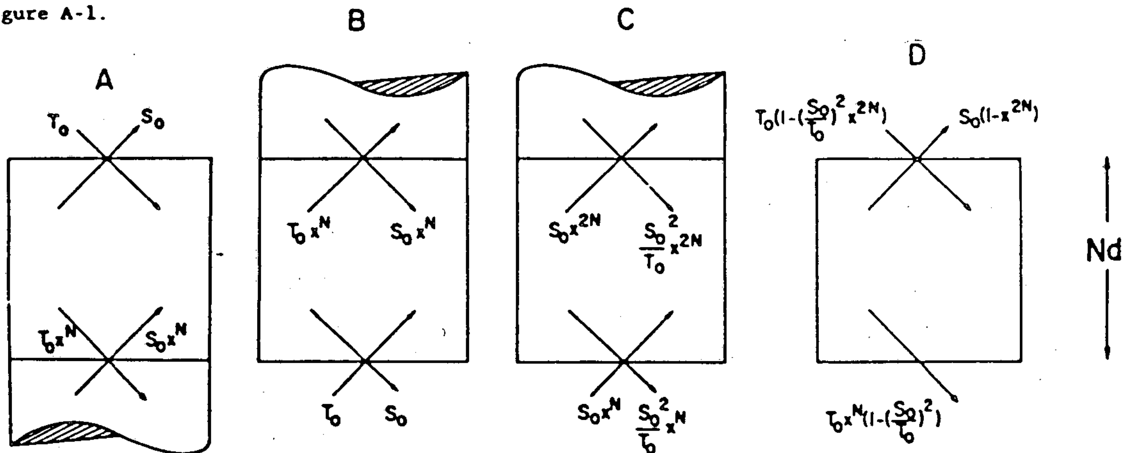

Finally, by dividing each amplitude in (D) by the incident amplitude, $T_0(1 - (S_0/T_0)^2x^{2N})$ we obtain the amplitude ratio for finite multilayer reflection and for finite multilayer transmission as was given in Eq. (4) and (5), viz.,

$$S_{0N}/T_0 = (S_0/T_0)\ (1-x^{2N})/(1-(S_0/T_0)^2x^{2N})$$

and

$$T_{0N}/T_0 = [1-(S_0/T_0)^2]x^N/(1-(S_0/T_0)^2x^{2N})$$

These analytical results combined with Eq. (1) above are accurate, adaptible and with an appreciably higher computational speed and ease of programming than that of the usual optical E&M (OEM) methods and may be applied with a small laboratory computer having complex number arithmetic capability.

The equivalence of the MDP and the OEM models for low energy x-rays has been demonstrated here by detailed comparisons plots (shown in Figs. 3-5). In recent reports by Lee (22) and by Perkins and Knight (23) the equivalence of the DP difference equation and the OEM approaches has been demonstrated by a formal rewriting of the latter into closed form. We are pleased to note that coincident with our presentation of the above derivation of the MDP results, Eqs. (4) and (5), Spiller and Rosenbluth (24) have presented their derivation of the same relations as developed from the OEM solution (see their Eqs. A13 and A14).

This MDP, phenomenological description which we have presented here can effectively provide the basis for a better understanding of the physical nature of multilayer reflection.

Finally, as noted earlier, we believe that our MDP model is more accurate at the higher photon energies (> 1000 eV) than the OEM model which does not include the angle-dependence of the scattered wave amplitudes which may be large for the shorter x-ray wavelengths. As discussed earlier, it is straightforward to distinguish between forward and 2θ-scattering in the MDP solution by inserting angle-dependent atomic scattering factors using a simple form factor correction (15).

ACKNOWLEDGEMENTS

The authors gratefully acknowledge the important assistance of other members of this Low Energy X-Ray Physics and Technology Project, Robert Ehrlich, Debra Nanod and Laureen Sasaki; and Mary Hockaday (of the P14 group, Los Alamos National Laboratory) for her helpful suggestions in preparation of this report. This program is supported by a grant from the Air Force Office of Scientific Research (AFOSR-No. 84-0001) and supplementally by contracts with the Department of Energy (SAN # CID #9501, Task 1) via LANL and LLNL (No. DE-AC03-76SF00098) via LBL.

REFERENCES

1. B.L. Henke, H.T. Yamada, and T.J. Tanaka, "Pulsed Plasma Source Spectrometry in the 80-8000 eV X-Ray Region," Rev. Sci. Instrum. 54, 1311 (1983).

2. B.L. Henke and P.A. Jaanimagi, "Two-Channel, Elliptical Analyzer Spectrograph for Absolute, Time-Resolving, Time-Integrating Spectrometry of Pulsed X-Ray Sources in the 100-10,000 eV Region" (Rev. Sci. Instrum., 56, 1537 (1985).

3. T.W. Barbee, Jr., S. Mrowka and M.C. Hettrick, "Molybdenum-silicon multilayer mirrors for the extreme ultraviolet," Appl. Opt. 24, 883 (1985).

4. E. Spiller, "Evaporated Multilayer Dispersion Elements for Soft X-Rays," AIP Conference Proceedings No. 75 on Low-Energy X-Ray Diagnostics, Monterey, California, edited by D.T. Attwood and B.L. Henke (American Institute of Physics, New York, 1965), 124.

5. L. Contardi, S.S. Chao, J. Keem, and J. Tyler, "Detection of Nitrogen with a Layered Structure Analyzer in a Wavelength Dispersive X-ray Microanalyzer," Scanning Electron Microscopy, 577 (1984).

6. A.E. Rosenbluth, "Reflecting Properties of X-Ray Multilayer Devices," Thesis, U. Rochester (1982).

7. J.H. Underwood and T.W. Barbee, Jr., "Layered Synthetic Microstructures as Bragg Diffractors for X-rays and Extreme Ultraviolet: Theory and Predicted Performance," Appl. Opt. 20, 3027 (1981).

8. J.H. Underwood and T.W. Barbee, Jr., "Synthetic Multilayers as Bragg Diffractors for X-rays and Extreme Ultraviolet: Calculations of Performance," AIP Conference Proceedings No. 75 on Low-Energy X-Ray Diagnostics, Monterey, California, edited by D.T. Attwood and B.L. Henke (American Institute of Physics, New York, 1965), 170.

9. A.H. Compton and S.K. Allison, X-Rays in Theory and Experiment, 2nd ed. (Van Norstrand, New York, 1935).

10. R.W. James, The Optical Principles of Diffraction of X-Rays (Cornell University Press, Ithaca, New York, 1965).

11. B.L. Henke and M.A. Tester, "Techniques of Low-Energy X-Ray Spectroscopy," Adv. X-Ray Anal. 18, 76 (1975).

12. B.L. Henke, R.C.C. Perera, E.M. Gullickson and M.L. Schattenburg, "High-Efficiency Low-Energy X-Ray Spectroscopy in the 100-500 eV Region," J. Appl. Phys. 49, 480 (1978).

13. L.A. Smirnov, T.D. Sotnikova, B.S. Anokhin, and B.Z. Taibin, "Total External Reflection of X-Rays from Rough Surfaces," Opt. Spectrosc. 46, 329 (1979).

14. K.D. Rachocki, D.R. Brown, R.W. Springer, and P.N. Arendt, "Auger and Depth Profile Analysis of Synthetic Crystals for Dispersion of Soft X-Rays," Applications of Surface Science 18, 165 (1984).

15. B.L. Henke, P. Lee, T.J. Tanaka, R.L. Shimabukuro, and B.K. Fujikawa, "Low-Energy X-Ray Interaction Coefficients: Photoabsorption, Scattering and Reflection," Atomic Data and Nuclear Data Tables 27, No. 1, (1982).

16. J.M. Auerbach and K.G. Tirsell, UCRL Report No. 91230.

17. D.M. Barrus, R.L. Blake, H. Felthauser, E.E. Fenimore, and A.J. Burek, "Spectrometric Properties of Crystals for Low-Energy X-Ray Diagnostics," AIP Conference Proceedings No. 75 on Low Energy X-Ray Diagnostics, Monterey, California, edited by D.T. Attwood and B.L. Henke (American Institute of Physics, New York, 1965), 115.

18. *LSM 83-021 Constructed by T. Barbee for the P-14 X-Ray Diagnostics Group, Los Alamos National Laboratory. LANL-P14 have also kindly loaned to us for this evaluation a W/C multilayer of the same d-spacing, #OVLA 070B-2 constructed by Energy Conversion Devices, Inc. These multilayers have essentially the same reflectivity characteristics.

19. B.L. Henke, "Low-Energy Interactions: Photoionization, Scattering, Specular and Bragg Reflection," AIP Conference Proceedings No. 75 on Low Energy X-Ray Diagnostics, Monterey, California, edited by D.T. Attwood and B.L. Henke (American Institute of Physics, New York, 1965), 146.

20. B.L. Henke, "Low-Energy X-Ray Spectroscopy with Crystals and Multilayers," AIP Conference Proceedings No. 75 on Low Energy X-Ray Diagnostics, Monterey, California, edited by D.T. Attwood and B.L. Henke (American Institute of Physics, New York, 1965), 85.

21. #Pb-Str (6-5-85 F3) constructed in this laboratory (See Ref's. 11 and 19).

22. P. Lee, "X-Ray Diffraction in Multilayers," Opt. Commun. 37, 159 (1981).

23. R.T. Perkins and L.V. Knight, "An Exact Analytic Solution of Darwin's Difference Equations," Acta Cryst. A40, 617 (1984).

24. E. Spiller and A.E. Rosenbluth, "Determination of Thickness Errors and Boundary Roughness from the Performance of a Multilayer Coating," Proceedings of SPIE - The International Society for Optical Engineering, Vol. 563, 221 (1985).

This report was done with support from the Department of Energy. Any conclusions or opinions expressed in this report represent solely those of the author(s) and not necessarily those of The Regents of the University of California, the Lawrence Berkeley Laboratory or the Department of Energy.

Reference to a company or product name does not imply approval or recommendation of the product by the University of California or the U.S. Department of Energy to the exclusion of others that may be suitable.

LAWRENCE BERKELEY LABORATORY
TECHNICAL INFORMATION DEPARTMENT
UNIVERSITY OF CALIFORNIA
BERKELEY, CALIFORNIA 94720